Challenging bulk viscous unified scenarios with cosmological observations

Weiqiang Yang,[1,*] Supriya Pan,[2,†] Eleonora Di Valentino,[3,‡] Andronikos Paliathanasis,[4,§] and Jianbo Lu[1,‖]

[1]*Department of Physics, Liaoning Normal University, Dalian 116029, P. R. China*
[2]*Department of Mathematics, Presidency University, 86/1 College Street, Kolkata 700073, India*
[3]*Jodrell Bank Center for Astrophysics, School of Physics and Astronomy, University of Manchester, Oxford Road, Manchester M13 9PL, United Kingdom*
[4]*Institute of Systems Science, Durban University of Technology, PO Box 1334, Durban 4000, Republic of South Africa*

(Received 30 June 2019; published 14 November 2019)

In a spatially flat Friedmann-Lemaître-Robertson-Walker universe, we investigate a unified cosmic fluid scenario endowed with bulk viscosity in which the coefficient of the bulk viscosity has a power law evolution. The power law in the bulk viscous coefficient is a general case in this study which naturally includes several choices as special cases. Considering such a general bulk viscous scenario, in the present work, we have extracted the observational constraints using the latest cosmological datasets and examine their behavior at the level of both background and perturbations. From the observational analyses, we find that a nonzero bulk viscous coefficient is always favored and some of the models in this series are able to weaken the current tension on H_0 for some dataset. However, from the Bayesian evidence analysis, Λ cold dark matter is favored over the bulk viscous model.

DOI: 10.1103/PhysRevD.100.103518

I. INTRODUCTION

Observational evidences from a series of distinct astronomical sources firmly state that nearly 96% of the total energy budget of the Universe is comprised of the dark sector [1]. This dark sector is usually classified into dark matter and the dark energy, in which the dark matter is responsible for the structure formation of the Universe and dark energy is speeding up the expansion of the Universe in an accelerating manner. The simplest possibility to model such a dark universe has been proposed in terms of the noninteracting ΛCDM cosmology in which $\Lambda > 0$, the cosmological constant, plays the role of dark energy and the dark matter sector is comprised with cold dark matter (CDM). However, the problems related to the cosmological constant have motivated the construction of alternative cosmological models. This has resulted in a class of cosmological models in which either the dark fluids evolve separately (known as noninteracting cosmological models) or the dark fluids have a mutual interaction between them, known as interacting dark energy models (see Refs. [2,3] for reviews on a class of noninteracting and interacting dark energy models). However, in spite of many investigations, the origin, nature, and the evolution of these dark fluids have been absolutely unknown until today.

Along the same line of investigation, a possible and natural idea in such a context is that the dark fluids, namely, the dark matter and dark energy, are not two exotic matter components but rather they are just two different aspects of a single fluid model, usually known as the *unified dark matter* (UDM) scenarios. Theoretically, there is no objection to considering such UDM scenarios since the nature of dark sector could be anything. In the context of Einstein's gravitational theory, such UDM scenarios are described by an equation of state $p = f(\rho)$, where p and ρ are, respectively, the pressure and energy density of the UDM fluid and f is any analytic function of the energy density, ρ (one can quickly recall the Chaplygin gas [4–15] and other unified cosmologies [16–18] in this context). Sometimes, these UDM scenarios are also studied in the form of $p = g(H)$, where g is any analytic function of H, the Hubble rate of the Friedmann-Lemaître-Robertson-Walker (FLRW) universe which is the well-known geometrical description of our Universe in the large scale, and in this present work we have considered such a geometrical configuration. However, one can see that the prescriptions, $p = f(\rho)$ and $p = g(H)$, are actually equivalent for a spatially flat universe since $\rho \propto H^2$ for this Universe; however, for nonflat cases, this equivalency does not hold. Thus, in a spatially at FLRW universe, one could either consider $p = f(\rho)$ or $p = g(H)$ to study the the UDM scenarios, keeping in mind that the respective function

*d11102004@163.com
†supriya.maths@presiuniv.ac.in
‡eleonora.divalentino@manchester.ac.uk
§anpaliat@phys.uoa.gr
‖lvjianbo819@163.com

should be analytic with respect to its argument, for instance ρ or H. A class of cosmological scenarios with this equation of state has been investigated in detail in the context of cosmological bulk viscosity [19–54] (also see Ref. [55] for a recent review on bulk viscous cosmologies). A bulk viscous fluid is a cosmic fluid endowed with bulk viscosity. Effectively, a bulk viscous fluid with (p,ρ) as, respectively, the pressure and energy density is identified with an effective pressure $p_{\rm eff}=(\gamma-1)\rho-\eta(\rho)u^{\mu}_{;\mu}$, in presence of the bulk viscosity.[1] Here, $u^{\mu}_{;\mu}$ is the expansion scalar of this fluid, $\eta(\rho)>0$ is the coefficient of the bulk viscosity, and γ is the model parameter. One can identify γ as a conventional equation of state of the fluid in the absence of the bulk viscosity. For a FLRW universe, $u^{\mu}_{;\mu}=3H$; hence, the effective pressure of the bulk viscous fluid in this Universe turns out to be $p_{\rm eff}=(\gamma-1)\rho-3H\eta(\rho)$. In Refs. [19–23,37,39,41], the viscous coefficient was taken to be $\eta(\rho)=\alpha\rho^m$, where α and m are free parameters and cosmic expansion was investigated in detail, but all the above works were mostly theoretical, both at background and perturbations. Concerning the observational examinations, although the low redshift data like supernovae type Ia have been used to constrain such bulk viscous models, but the full cosmic microwave background (CMB) temperature and anisotropy data (we acknowledge that CMB shift parameter was introduced in Ref. [41]), so far we are aware of the literature, have not been applied to such models. Thus, we believe that such an analysis will be worth for a better understanding of such scenarios.

Thus, to take into account the observational features of bulk viscous models, in the present work, we have considered two specific UDM scenarios and constrained them using different cosmological data. We have also studied the evolution of these models at the level of perturbations through the temperature anisotropy in the CMB spectra and matter power spectra as well.

The work is organized in the following manner. In Sec. II, we present the gravitational field equations for an imperfect fluid with bulk viscosity. In Sec. III, we present the observational data and the constraints of the present models. In particular, in the Secs. III A and III B, we summarize the main results of the two models, respectively. Finally, we close the present work in Sec. IV with a brief summary.

II. BACKGROUND AND PERTURBATION EQUATIONS FOR A VISCOUS UNIVERSE

We consider a homogeneous and isotropic model of our Universe, which is characterized by the usual Friedmann-Lemaître-Robertson-Walker line element

$$ds^2=-dt^2+a^2(t)\left[\frac{dr^2}{1-kr^2}+r^2(d\theta^2+\sin^2\theta d\phi^2)\right],$$

where $a(t)$ is the scale factor of the Universe; k is the spatial curvature, its three distinct values of which, namely, 0, -1, and $+1$, represent a spatially flat, open, and closed universe, respectively. In this work, we shall confine ourselves to the spatially flat universe, which means $k=0$ throughout the work. The energy density, ρ, of the universe in this spacetime is thus constrained by the Hubble rate $H\equiv\dot{a}/a$ as ($8\pi G=1$)

$$3H^2=\rho_t=(\rho_r+\rho_b+\rho_D), \tag{1}$$

where ρ_r, ρ_b, and ρ_D are, respectively, the energy density for the radiation and baryons and the unified fluid where $p_D=(\gamma-1)\rho_D$ and we have a bulk viscosity background. Following Ref. [20], the effective pressure of the unified dark fluid can be written as

$$p_{\rm eff}=p_D-3H\eta(\rho_D), \tag{2}$$

where $\eta(\rho_D)$ is the coefficient of the bulk viscosity that we assume to take the following well-known form [19–21]:

$$\eta(\rho_D)=\alpha\rho_D^m, \qquad (\alpha>0). \tag{3}$$

Thus, the effective pressure for the unified dark fluid can be recast into

$$p_{\rm eff}=(\gamma-1)\rho_D-3\alpha H\rho_D^m. \tag{4}$$

In the spatially flat universe, at late time, the contributions from radiation and baryons are negligible, so, approximately, $H\propto\rho_D^{1/2}$, and this is equivalent to a total stress of the form $p_{\rm eff}\approx(\gamma-1)\rho_D-\sqrt{3}\alpha\rho_D^{m+1/2}$ [19–21], where this equation reduces to the generic form $p_{\rm eff}+\rho_D\approx\Gamma\rho_D^{\delta}$ with $\gamma=0$ and $\delta=m+1/2$ and $\Gamma=-\sqrt{3}\alpha$. For these kinds of effective pressure of the dark fluid, there are three free model parameters, γ, α, and m. The pressure $p_{\rm eff}=-3\alpha H\rho_D^m$ with assuming $\gamma=1$, and we can define the dimensionless parameter $\beta=\alpha H_0\rho_{t0}^{m-1}$, where ρ_{t0} is the present value of ρ_t defined in Eq. (1). Let us note that the model with $p_{\rm eff}=-3\alpha H\rho_D^m$ was constrained by the supernovae type Ia [71] and CMB shift-parameter [72] data in which the best-fit values of the parameters were found to be $m=-0.4$ and $\beta=0.236$.

In the present work, we seek a robust observational analysis of the bulk viscous cosmologies [19–23,41] in a spatially flat universe. Thus, in the presence of the bulk viscosity, the effective pressure of the unified fluid becomes

$$p_{\rm eff}=(\gamma-1)\rho_D-\sqrt{3}\alpha\rho_t^{1/2}\rho_D^m, \tag{5}$$

[1]In this connection we recall an equivalent cosmological theory known gravitationally induced particle creation theory [56–69] which is equivalent to the bulk viscous theory at the level of equations but from the thermodynamical point of view both are theories are distinct [70].

where the baryons and radiation components present in ρ_t [see Eq. (1)] are conserved separately, and hence they evolve as $\rho_b = \rho_{b0}a^{-3}$ and $\rho_r = \rho_{r0}a^{-4}$, respectively. Here, the energy density of viscous dark fluid would not be in an analytical form due to the baryons and radiation in the effective pressure; however, it could be solved numerically. The effective equation of state of viscous dark fluid will be

$$w_{\rm eff} = (\gamma - 1) - \sqrt{3}\alpha\rho_t^{1/2}\rho_D^{m-1}. \tag{6}$$

The adiabatic sound speed for the viscous fluid is

$$c^2_{a,\rm eff} = \frac{p'_{\rm eff}}{\rho'} = w_{\rm eff} + \frac{w'_{\rm eff}}{3\mathcal{H}(1+w_{\rm eff})}, \tag{7}$$

where the prime denotes the derivative of the conformal time. $\mathcal{H}$ is the conformal Hubble parameter, $\mathcal{H} = aH$.

When the equation of state of a purely barotropic fluid is negative, it has an imaginary adiabatic sound speed, which possibly causes instability of the perturbations. To avoid this problem, we will allow an entropy perturbation (nonadiabatic perturbation) in the dark fluid according to the analysis of generalized dark matter [73].

To follow the analysis of entropy perturbation for a generalized dark matter [73], in the entropy perturbation mode, the true pressure perturbation is from the effective pressure, and $p_{\rm eff} = p_D - 3H\eta(\rho_D)$ is from $p_{\rm eff} = p_D - \eta(\nabla_\sigma u^\sigma)$, so one could calculate the pressure perturbation

$$\begin{aligned}\delta p_{\rm eff} &= \delta p_D - \delta\eta(\nabla_\sigma u^\sigma) - \eta(\delta\nabla_\sigma u^\sigma)\\ &= \delta p_D - 3H\delta\eta - \frac{\eta}{a}\left(\theta + \frac{h'}{2}\right).\end{aligned} \tag{8}$$

Combined with $\eta = \alpha\rho_D^m$ [20,21], the effective sound speed of viscous dark fluid could be defined as

$$\begin{aligned}c^2_{\rm s,eff} &\equiv \left.\frac{\delta p_{\rm eff}}{\delta\rho_D}\right|_{rf}\\ &= c_s^2 - \sqrt{3}\alpha m\rho_t^{1/2}\rho_D^{m-1} - \frac{\alpha\rho_D^{m-1}}{a\delta_D}\left(\theta + \frac{h'}{2}\right),\end{aligned} \tag{9}$$

where $|_{rf}$ denotes the rest frame, generally the sound speed $c_s^2 = 0$ in the rest frame according to the analysis of Ref. [73].

To follow the formalism for a generalized dark matter [73], one can write the perturbation equations of density contrast and velocity divergence

$$\begin{aligned}\delta'_D &= -(1+w_{\rm eff})\left(\theta_D + \frac{h'}{2}\right) + \frac{w'_{\rm eff}}{1+w_{\rm eff}}\delta_D\\ &\quad - 3\mathcal{H}(c^2_{\rm s,eff} - c^2_{a,\rm eff})\left[\delta_D + 3\mathcal{H}(1+w_{\rm eff})\frac{\theta_D}{k^2}\right],\end{aligned} \tag{10}$$

$$\theta'_D = -\mathcal{H}(1 - 3c^2_{\rm s,eff})\theta_D + \frac{c^2_{\rm s,eff}}{1+w_{\rm eff}}k^2\delta_D, \tag{11}$$

Now, based on the effective pressure of the viscous dark fluid model [19–21], we consider two bulk viscous fluid models, namely, the model with two free parameters α and m, labeled as BVF1, and another model with three parameters γ, α, and m, labeled as BVF2. Let us note that for the BVF1 and BVF2 models for the purpose of statistical analysis, we have turned α into a a dimensionless quantity by defining $\beta = \alpha\rho_0^{m-1/2}$ in terms of the original parameter α. Thus, from now on, we shall recognize β and m as the governing parameters of model BVF1, and the model BVF2 will be recognized by the parameters β, γ, and m. The case with $m = 0$ is the simplest bulk viscous scenario representing the constant bulk viscosity. Thus, in the present work, we consider four different bulk viscous scenarios as follows: the two cases with $m = 0$, which means we consider two different scenarios, namely, BVF1 ($m = 0$) and BVF2 ($m = 0$), and, second, we consider the general scenarios in which m acts as a free parameter, which means the two cases for free m, named BVF1 (m: free) and BVF2 (m: free). Now, to understand the qualitative evolution of the density parameters for radiation, baryons, and the effective bulk viscous fluid, we have systematically investigated all the possibilities. In Fig. 1, we have shown the density parameters for the model BVF1 ($m = 0$) using different values of β such as $\beta = 0.5$ (upper panel of Fig. 1), $\beta = 0.55$ (middle panel of Fig. 1), and $\beta = 0.6$ (lower panel of Fig. 1). From this figure (Fig. 1), we see that as β increases the domination of the bulk viscous fluid starts lately. Now, to understand the general scenario with free m, in Fig. 2, we have depicted two different scenarios for the density parameters for some fixed values of β and m. In a similar fashion, we have investigated the qualitative evolution of the density parameters for BVF2 considering both the possibilities, which means the case with $m = 0$ (see Fig. 3) and with free m (see Fig. 4). From the qualitative evolution of various bulk viscous models presented in the aforementioned figures, one can easily notice that the dynamics associated with $\beta = 0$ is problematic since for $\beta = 0$ one can see that (see Figs. 1 and 3) at early times radiation was more subdominated than the bulk viscous fluid, which is impossible. However, the above discussions imply that β should be greater than zero in order to have realistic bulk viscous scenarios.

III. OBSERVATIONAL DATA AND THE RESULTS

In this section, we describe both the observational data and the analyses of the present bulk viscous scenarios. In what follows, we first describe the observational datasets:

(i) *Cosmic microwave background.*—CMB radiation is the effective astronomical probe to analyze the

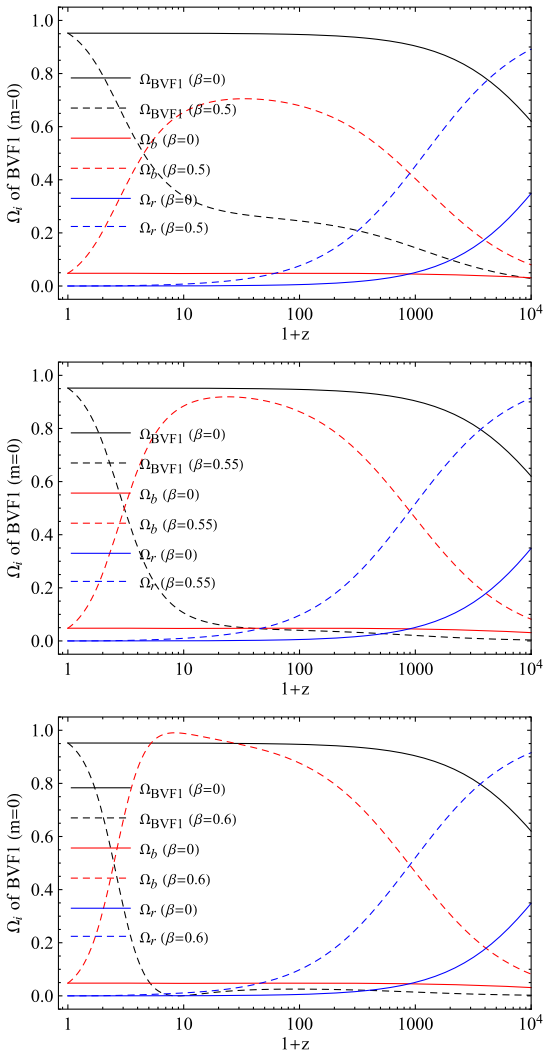

FIG. 1. Qualitative evolution of the density parameters for the BVF1 model with $m = 0$ is shown for different values of β, namely, $\beta = 0.5$ (upper panel), $\beta = 0.55$ (middle panel), and $\beta = 0.6$ (lower panel), and also compared with the no bulk viscous scenario (corresponding to $\beta = 0$).

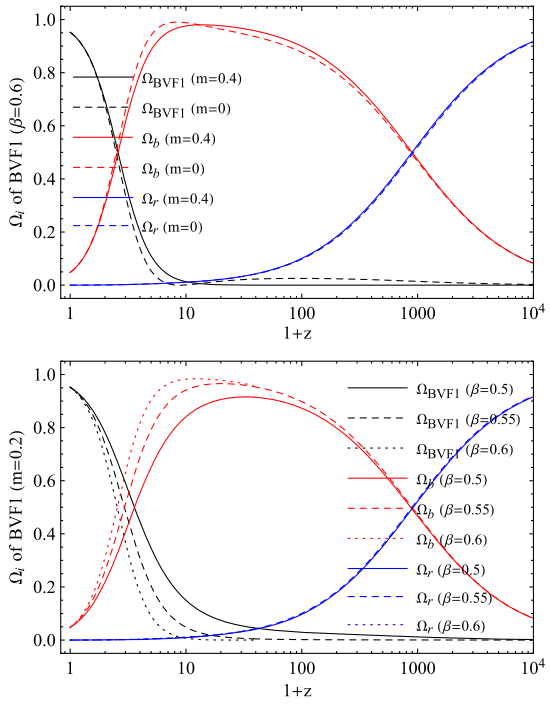

FIG. 2. We show some general behavior of the BVF1 model, considering the fact that $m \neq 0$. In the upper panel, we fix $\beta = 0.6$ and consider the density parameters for $m = 0.4$ and also compare to the constant bulk viscous scenario (corresponding to $m = 0$). In the lower panel, we fix $m = 0.2$ and consider three different values of β in order to depict the evolution of the density parameters.

dark energy models. Here, we consider the CMB temperature and polarization anisotropies together with their cross-correlations from Planck 2015 [74]. Particularly, we consider the combinations of high- and low-ℓTT likelihoods in the multipoles range $2 \leq \ell \leq 2508$ and the combinations of the high- and low-ℓ polarization likelihoods as well as Ref. [75].

(ii) *Pantheon sample from the supernovae type Ia data.*—We use the most recent compilation of the supernovae type Ia comprising 1048 data points [76] in the redshift range $z \in [0.01, 2.3]$.

(iii) *Hubble parameter measurements.*—Finally, we consider the Hubble parameter values at different redshifts measured from the cosmic chronometers (CCs). The CCs are the most massive and passively evolving galaxies in the Universe. For a detailed motivation and measurements of the Hubble parameter values from CCs, we refer to Ref. [77]. In this work, we consider 30 measurements of the Hubble parameter values spread in the interval $0 < z < 2$; see again Ref. [77], in which the data points are tabulated.

Now, to constrain the bulk viscous scenarios, we have made use of the fastest algorithm, the Markov chain Monte Carlo package cosmomc [78] in which an efficient convergence diagnostic, namely, the Gelman-Rubin criteria $R - 1$ [79], which enables us to understand the convergence of the Monte Carlo chains, exists. For the first model BVF1, the analyzed parameters space is $\mathcal{P}_{\rm BVF1} = \{\Omega_b h^2, 100\theta_{MC}, \tau, n_s, \ln(10^{10}A_s), \beta, m\}$, and for the second model BVF2, the parameters space is $\mathcal{P}_{\rm BVF2} = \{\Omega_b h^2, 100\theta_{MC}, \tau, n_s, \ln(10^{10}A_s), \beta, m, \gamma\}$, where $\Omega_b h^2$ is the baryon density, $100\theta_{MC}$ is the ratio of the sound horizon to the angular diameter distance, τ is the optical depth, n_s is the scalar spectral index, and A_S is the amplitude of the initial power spectrum. In Table I, we summarize the priors on the model parameters that have been used during the statistical analysis. Let us now analyze the results of the models extracted from the observational datasets.

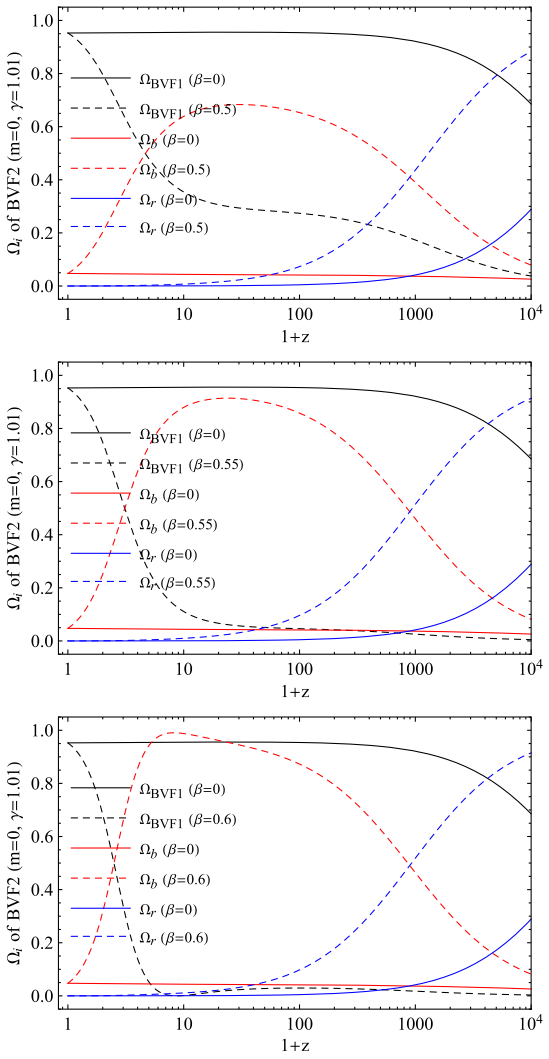

FIG. 3. Qualitative evolution of the density parameters for the BVF2 model with $m = 0$ is shown for different values of β, namely, $\beta = 0.5$ (upper panel), $\beta = 0.55$ (middle panel), and $\beta = 0.6$ (lower panel), and is also compared with the no bulk viscous scenario (corresponding to $\beta = 0$). Let us note that for all the plots we have fixed $\gamma = 1.01$.

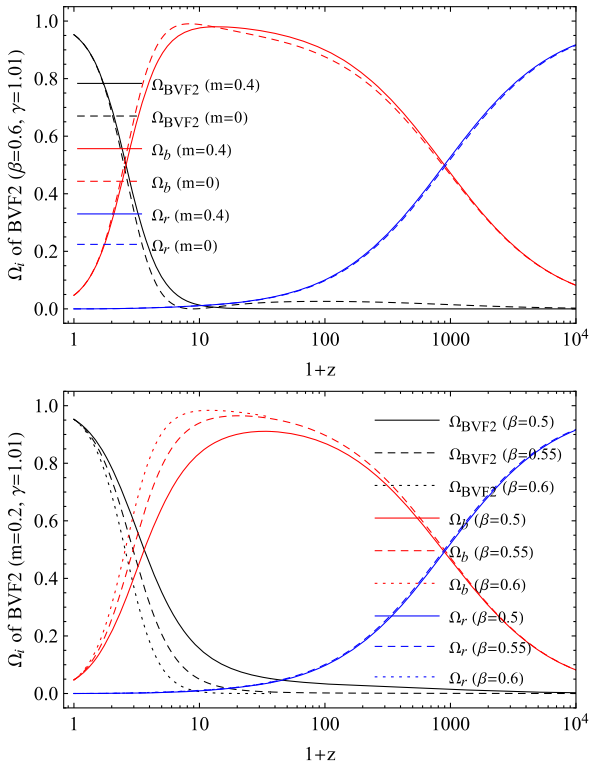

FIG. 4. We show some general behavior of the BVF2 model considering the fact that $m \neq 0$. In the upper panel, we fix $\beta = 0.6$ and consider the density parameters for $m = 0.4$ and also compared to the constant bulk viscous scenario (corresponding to $m = 0$). In the lower panel, we fix $m = 0.2$ and consider three different values of β in order to depict the evolution of the density parameters. Let us note that for all the plots we have fixed $\gamma = 1.01$.

A. Model BVF1

Here, we present the observational summary of the BVF1 model using various combinations of the cosmological datasets. The governing parameters of this model, as already mentioned, are m and β (we recall again that $\beta = \alpha\rho_{t0}^{m-1/2}$). We first consider the simplest bulk viscous scenario with $m = 0$ that represents a constant bulk viscosity in the Universe sector and then proceed toward the more general scenario in which m has been taken to be a free parameter.

For the scenario with $m = 0$, we have constrained the model using four different observational datasets, namely, CMB, CMB + CC, CMB + Pantheon, and CMB + Pantheon + CC, and the results of the scenario are summarized in Table II. From Table II, one may notice that the results can be divided in two different blocks, with and without Pantheon, while they are about insensitive to the presence of CCs. In particular, we see that adding Pantheon we have a shift of all the cosmological parameters, except θ_{MC}, toward higher values. Moreover, one can see that here for θ_{MC} and H_0 the CMB case goes down several standard deviations, about 20, compared to the

TABLE I. We show the priors on the free parameters of the bulk viscous scenarios.

Parameter	Prior
$\Omega_b h^2$	[0.005, 0.1]
$\Omega_c h^2$	[0.01, 0.99]
τ	[0.01, 0.8]
n_s	[0.5, 1.5]
$\log[10^{10}A_s]$	[2.4, 4]
$100\theta_{MC}$	[0.5, 10]
β	[0, 1]
m	$[-2, 0.5]$
γ	$[-3, 3]$

TABLE II. 68% and 95% C.L. constraints on various free parameters of the model BVF1 assuming the simplest case $m = 0$, which means the constant bulk viscosity, using different observational data. Here, H_0 is in the units of km/Mpc/ sec.

Parameters	CMB	CMB + CC	CMB + Pantheon	CMB + Pantheon + CC
$\Omega_b h^2$	$0.02222^{+0.00015+0.00029}_{-0.00014-0.00029}$	$0.02227^{+0.00016+0.00031}_{-0.00017-0.00031}$	$0.02251^{+0.00016+0.00030}_{-0.00015-0.00030}$	$0.02256^{+0.00015+0.00031}_{-0.00017-0.00030}$
$100\theta_{MC}$	$1.03329^{+0.00028+0.00055}_{-0.00028-0.00057}$	$1.03332^{+0.00028+0.00055}_{-0.00027-0.00053}$	$1.03325^{+0.00027+0.00052}_{-0.00026-0.00053}$	$1.03327^{+0.00029+0.00061}_{-0.00033-0.00057}$
τ	$0.077^{+0.016+0.033}_{-0.016-0.032}$	$0.080^{+0.019+0.031}_{-0.017-0.033}$	$0.097^{+0.019+0.035}_{-0.018-0.034}$	$0.099^{+0.017+0.032}_{-0.017-0.033}$
n_s	$0.9640^{+0.0043+0.0088}_{-0.0044-0.0085}$	$0.9652^{+0.0044+0.0089}_{-0.0045-0.0083}$	$0.9741^{+0.0043+0.0085}_{-0.0043-0.0080}$	$0.9750^{+0.0043+0.0087}_{-0.0043-0.0081}$
$\ln(10^{10}A_s)$	$3.090^{+0.032+0.062}_{-0.032-0.062}$	$3.094^{+0.039+0.059}_{-0.031-0.065}$	$3.120^{+0.034+0.069}_{-0.035-0.066}$	$3.124^{+0.035+0.062}_{-0.033-0.066}$
β	$0.199^{+0.0041+0.0081}_{-0.0042-0.0084}$	$0.201^{+0.0045+0.0089}_{-0.0044-0.0092}$	$0.211^{+0.0044+0.0085}_{-0.0048-0.0080}$	$0.212^{+0.0040+0.0079}_{-0.0040-0.0075}$
H_0	$54.99^{+0.29+0.59}_{-0.30-0.59}$	$55.10^{+0.32+0.63}_{-0.31-0.65}$	$55.86^{+0.32+0.63}_{-0.35-0.59}$	$55.95^{+0.30+0.60}_{-0.33-0.56}$
$\chi^2_{\text{best-fit}}$	12962.552	12991.452	14137.924	14163.750

Planck's ΛCDM-based estimation [1]. This is a very striking result since the estimated values of θ_{MC} and H_0 for $m = 0$ have large difference compared to their estimated values in ΛCDM based Planck's results [1], and the H_0 constraint is twice as strong as the ΛCDM one. On the other hand, the constant β assumes small values, and it is always different from zero at more than four standard deviations, which goes in favor of the bulk viscosity. In Fig. 5, we show the one-dimensional marginalized posterior distributions for some free parameters as well as the two-dimensional contour plots considering various dataset combinations for the BVF1 model. From this figure (i.e., Fig. 5), one can clearly see that the parameters are correlated with one another. In particular, there is a strong

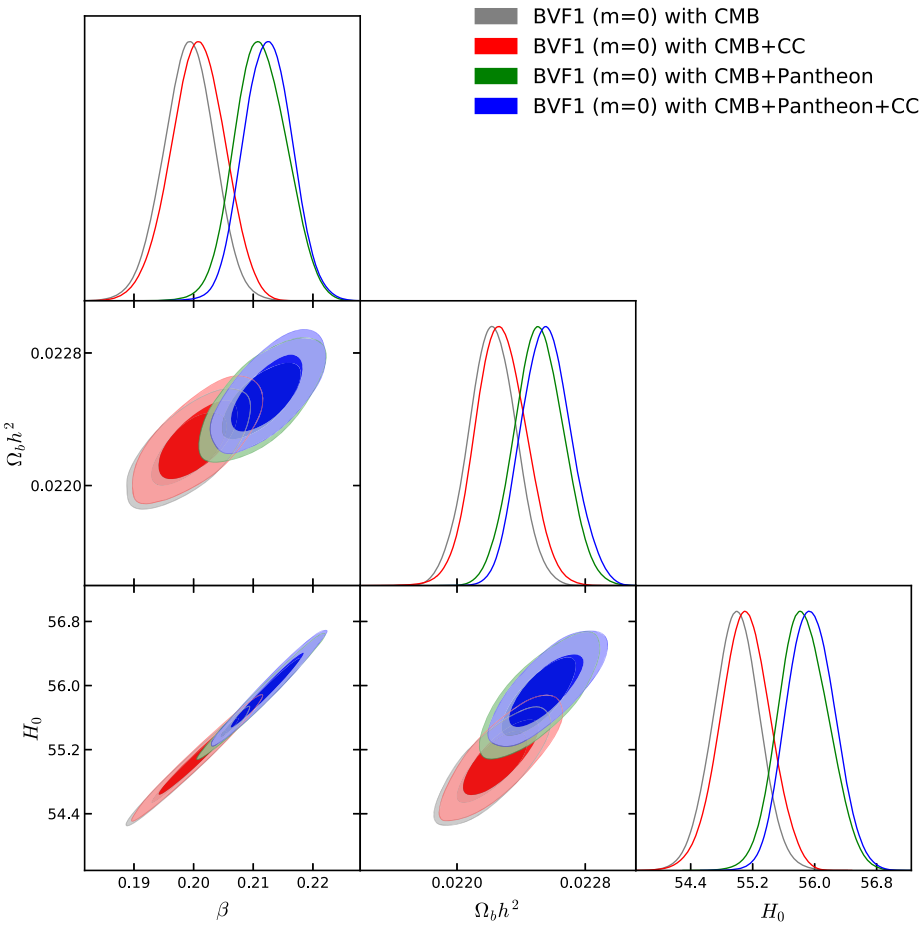

FIG. 5. 68% and 95% C.L. contour plots for the BVF1 model with $m = 0$, using the observational data from different sources. The figure also shows the one-dimensional marginalized posterior distributions for some selected parameters.

TABLE III. 68% and 95% C.L. constraints on various free parameters of the model BVF1 with m free using different observational data. Here, H_0 is in the units of km/Mpc/ sec.

Parameters	CMB	CMB + CC	CMB + Pantheon	CMB + Pantheon + CC
$\Omega_b h^2$	$0.02223^{+0.00015+0.00030}_{-0.00015-0.00030}$	$0.02223^{+0.00015+0.00030}_{-0.00015-0.00028}$	$0.02219^{+0.00015+0.00030}_{-0.00015-0.00031}$	$0.02220^{+0.00015+0.00031}_{-0.00015-0.00030}$
$100\theta_{MC}$	$1.0328^{+0.0046+0.0052}_{-0.0048-0.0057}$	$1.0293^{+0.00087+0.0019}_{-0.00097-0.0021}$	$1.02759^{+0.00057+0.0011}_{-0.00056-0.0011}$	$1.02759^{+0.00057+0.0011}_{-0.00056-0.0011}$
τ	$0.077^{+0.017+0.031}_{-0.017-0.033}$	$0.079^{+0.018+0.035}_{-0.018-0.036}$	$0.077^{+0.017+0.034}_{-0.018-0.033}$	$0.078^{+0.017+0.033}_{-0.017-0.034}$
n_s	$0.9646^{+0.0046+0.0095}_{-0.0047-0.0092}$	$0.9652^{+0.0049+0.0091}_{-0.0047-0.0092}$	$0.9652^{+0.0045+0.0091}_{-0.0046-0.0089}$	$0.9653^{+0.0044+0.0088}_{-0.0045-0.0088}$
$\ln(10^{10}A_s)$	$3.089^{+0.033+0.061}_{-0.033-0.064}$	$3.093^{+0.035+0.068}_{-0.034-0.070}$	$3.090^{+0.034+0.066}_{-0.034-0.063}$	$3.091^{+0.033+0.065}_{-0.034-0.065}$
β	$0.22^{+0.20+0.23}_{-0.18-0.20}$	$0.365^{+0.038+0.072}_{-0.029-0.066}$	$0.428^{+0.016+0.032}_{-0.016-0.034}$	$0.429^{+0.017+0.033}_{-0.016-0.033}$
m	$-0.06^{+0.40+0.44}_{-0.41-0.51}$	$-0.356^{+0.081+0.176}_{-0.088-0.194}$	$-0.544^{+0.066+0.13}_{-0.059-0.13}$	$-0.545^{+0.066+0.12}_{-0.058-0.12}$
H_0	56^{+11+13}_{-10-12}	$64.1^{+2.0+4.5}_{-1.9-3.9}$	$68.0^{+1.1+2.3}_{-1.1-2.3}$	$68.1^{+1.1+2.3}_{-1.2-2.2}$
$\chi^2_{\text{best-fit}}$	12957.848	12976.224	13997.658	14013.128

positive correlation among the parameters shown in the figure for this model.

Now, concerning the general scenario in which m acts as a free parameter, we have summarized the observational constraints on the model parameters in Table III at 68% and 95% C.L. From our analyses (see Table III), we see that the CMB data alone return a very low value of the Hubble parameter at present, i.e., $H_0 = 56^{+11}_{-10}$ at 68% C.L. but with large error bars, and of θ_{MC}, i.e., $100\theta_{MC} = 1.0328^{+0.0046}_{-0.0048}$. Subsequently, when the external datasets are added to the CMB, the error bars on H_0 significantly decrease, and H_0 increases. We see that the addition of CCs to the CMB gives better constraints on H_0 and θ_{MC}, contrary to the results with respect to the $m = 0$ case. However, the best constraints are achieved for the addition of the Pantheon data to the CMB, and the results for this dataset (i.e., CMB + Pantheon) are practically indistinguishable from the full combination CMB + Pantheon + CC. Thus, to show the graphical variations for the model parameters, we limit to three combined analyses, namely, CMB + CC, CMB + Pantheon, and CMB + Pantheon + CC, because the CMB-only constraints are too large and the figure would be unreadable if added. In Fig. 6, for the above three datasets, we show the one-dimensional marginalized posterior distributions for the free parameters of the model as well as the two-dimensional contour plots for several combinations of the free parameters at 68% and 95% C.L. From this plot, we can see the strong anticorrelation between m and β. Moreover, from Fig. 6, we have some common features of some parameters that are independent of the datasets. We see that the parameter β has a strong positive correlation to H_0, and this is independent of the datasets used. Correspondingly, we find that the parameter m has a strong negative correlation to H_0. Further, one can notice that there is a notable shift between the constraints from CMB, CMB + CC, and CMB + Pantheon. For the dataset CMB + CC, the estimation of H_0 ($= 63.2^{+2.4}_{-1.6}$, 68% C.L.) moves toward a higher value with respect to the CMB alone but is still slightly far from the measurements by Planck [1] in the ΛCDM scenario, while for the dataset CMB + Pantheon, the estimated value of H_0 ($= 68.0 \pm 1.1$, 68% C.L.) is similar to Planck [1] but with slightly large error bars. Interestingly, one can notice that, due to large error bars on H_0 for this dataset (i.e., CMB + Pantheon), it is possible to weaken the tension on H_0 observed from the local estimation of H_0 measured by Riess *et al.* in 2016, $H_0 = 73.24 \pm 1.74$ km s^{-1} Mpc^{-1} [80], and in 2018, $H_0 = 73.48 \pm 1.66$ km s^{-1} Mpc^{-1} [81], under 3σ C.L. However, if we consider the updated value of the present-day Hubble constant, $H_0 = 74.03 \pm 1.42$ km s^{-1} Mpc^{-1} of Riess *et al.* in 2019 [82], the tension is still at 3.3σ. This is one of the interesting results in this context since the H_0 tension is partially alleviated, even if this is probably due to a volume effect, i.e., to the large error bars imposed by the observational data. On the contrary, with respect to the case with $m = 0$, the θ_{MC} parameter shifts toward lower values, moving away from Planck [1] in the ΛCDM scenario when adding CCs or the Pantheon to the CMB. Finally, for the last combination, which means CMB + Pantheon + CC, we find identical constraints compared to CMB + Pantheon, showing that CCs are not adding any new information to the analysis. A similar observation can be found from the constraints on the model parameters; specifically, looking at the constraints on m and β, we can see that the combinations CMB + CC, CMB + Pantheon, and CMB + Pantheon + CC significantly improve the parameter space compared to the constraints obtained only from the CMB data alone. In fact, while for the CMB case we have an indication at two standard deviations for β greater than zero, this becomes very robust evidence at several standard deviations after the inclusion of other cosmological probes. In particular, we have a shift toward higher values, passing from $\beta = 0.22^{+0.20}_{-0.18}$ at 68% C.L. for CMB alone, to $\beta = 0.350^{+0.042}_{-0.026}$ at 68% C.L. for CMB + CC, to $\beta = 0.428 \pm 0.016$ at 68% C.L. for CMB + Pantheon.

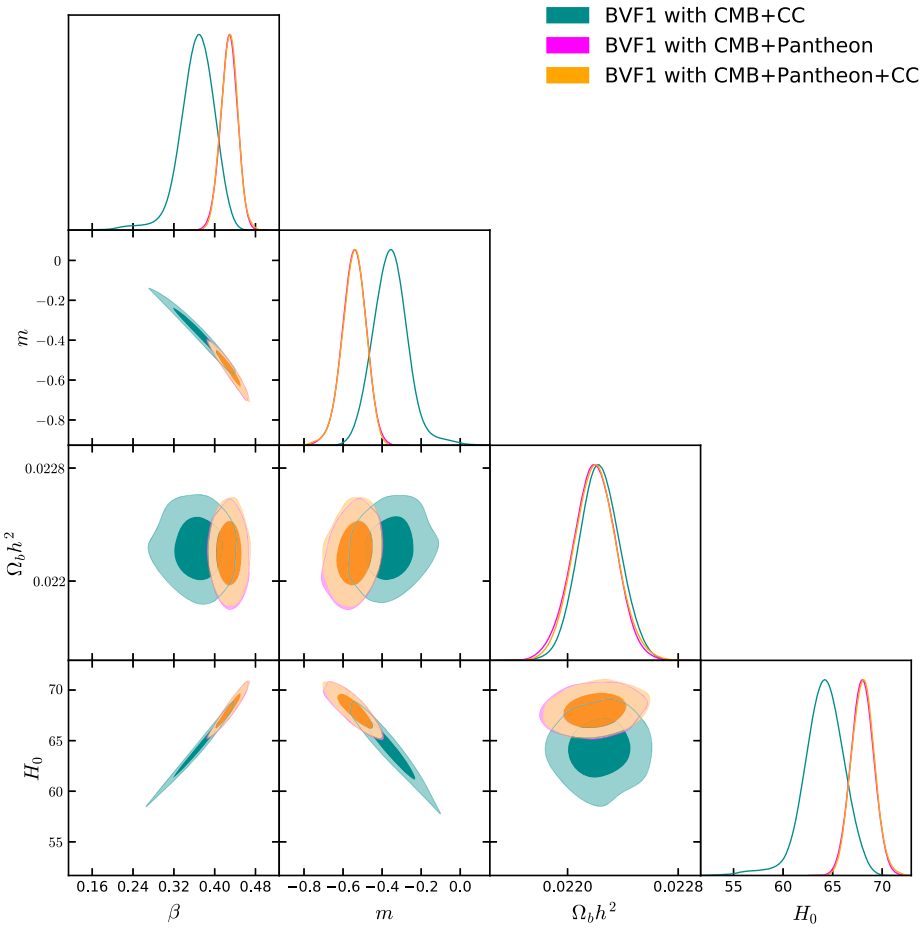

FIG. 6. The figure displays the 68% and 95% C.L. contour plots between various combinations of the parameters of the model BVF1 with m free using the observational data from different sources. The figure also shows the one-dimensional marginalized posterior distributions for some selected parameters.

Analogously, we see that due to the negative correlation between m and β, a shift in the parameter m towards its lower values is realized. This results in a solid evidence for m to be negative and different form zero at about roughly eight standard deviations for the full combination CMB + Pantheon + CC. Also, for this parameter, while the CMB-alone value is in agreement with $m = 0$ ($m = -0.06^{+0.40}_{-0.41}$ at 68% C.L.), it moves to $m = -0.320^{+0.073}_{-0.099}$ at 68% C.L. after the inclusion of CC and to $m = -0.544^{+0.066}_{-0.059}$ at 68% C.L. for CMB + Pantheon. If we compare Table II with $m = 0$ with Table III with m free, we see an exceptional gain of $\Delta\chi^2 = 150$, supporting the necessity of m being different from zero.

1. BVF1 model at large scales

We now discuss the behavior of the BVF1 model at the level of perturbations considering the direct impacts on the CMB TT spectra. We start with the constant bulk viscous scenario (i.e., $m = 0$) and display the CMB TT spectra in Fig. 7, using the best-fit values of all model parameters

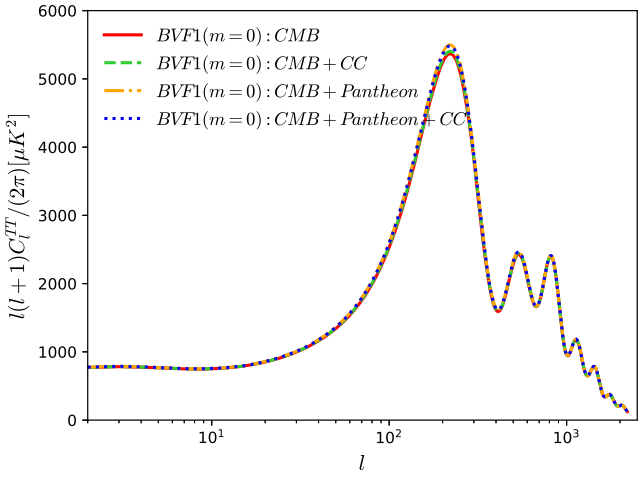

FIG. 7. CMB temperature power spectra using the best-fit values of various free and derived parameters are shown for the BVF1 model with $m = 0$ (i.e., the constant bulk viscosity).

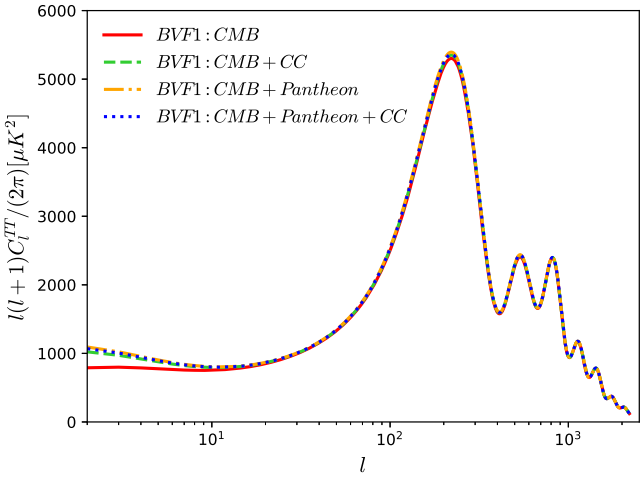

FIG. 8. CMB temperature power spectra using the best-fit values of various free and derived parameters of the generalized the bulk viscous model BVF1.

obtained for different observational datasets. From different spectrum corresponding to each observational data set, namely, CMB, CMB + CC, CMB + Pantheon, and CMB + Pantheon + CC, one cannot distinguish between them.

For the second scenario of this model with free m (i.e., model BVF2), we perform an investigation similar to that for BVF1 ($m = 0$). In Fig. 8, we show the CMB TT spectra for all the observational datasets using the best-fit values of the model parameters. We find that a difference in the lower multipoles (i.e., $l \leq 10$), i.e., in the cosmic variance limited region, exists between the TT curve for CMB alone dataset and the TT curves for the remaining observational datasets, while for higher multipoles (i.e., $l > 10$), we do not observe any changes in the curves.

B. Model BVF2

The main free parameters of this model are β, γ, and m. So, following a fashion similar to that performed with model BVF1, here, too, we consider the constant bulk viscosity scenario leading to $m = 0$ as the simplest possibility and then proceed toward the more general bulk viscous scenario assuming m to be a free parameter.

In Table IV, we show the observational constraints for the constant bulk viscous model (the $m = 0$ case) at the 68% and 95% C.L. From the Table IV, one can readily see that the error bars are strongly relaxed, until an order of magnitude, with respect to the BVF1 case. We also find in this BVF2 scenario a large shift of θ_{MC} at about five standard deviations and H_0 toward lower values, with respect to the ΛCDM model, but thanks to the larger error bars, now the shift is less significant. In particular, we have $H_0 = 56.1^{+3.4}_{-3.6}$ km/s/Mpc at 68% C.L for the dataset CMB only, to be compared to its estimation by Planck [1], $H_0 = 67.27 \pm 0.66$ km/s/Mpc at 68% C.L. When the external datasets, such as CC and Pantheon are added to the CMB, H_0 goes up (more in agreement with the ΛCDM value), and θ_{MC} goes down (increasing the disagreement with the ΛCDM value), and the error bars on them are also reduced compared to their estimation from CMB only. Moreover, γ shifts away from 1 (which corresponds to the BVF1 scenario) of several standard deviations when more datasets are combined together. For this model, contrary to the BVF1 case, the addition of the CC dataset improves the parameter constraints, although for the CMB + CC data, the estimated value of $H_0 = 60.8^{+1.9}_{-1.4}$ km/s/Mpc at 68% C.L. is still lower than Ref. [1]. When considering the Pantheon datasets and the full combination, namely, CMB + Pantheon and CMB + Pantheon + CC, the Hubble constant H_0 has the strongest constraints, and it shifts toward higher values. Therefore, it is quite interesting to notice that for the CMB + Pantheon dataset the tension in H_0 with the local measurements is clearly reconciled within 95% C.L., even considering the latest Riess *et al.* 2019 measurement [82]. For the full combination CMB + Pantheon + CC, the tension is also released, but within 3σ. Concerning the β parameter, we always find that it is different from zero at more than 95% C.L., irrespective of the observational datasets. We again note that for the CMB-only data β has the maximum error bars, which eventually decrease after the

TABLE IV. 68% and 95% C.L. constraints on various free parameters of the model BVF2 assuming the simplest case $m = 0$, which means the constant bulk viscosity, using different observational data. Here, H_0 is in units of km/Mpc/ sec.

Parameters	CMB	CMB + CC	CMB + Pantheon	CMB + Pantheon + CC
$\Omega_b h^2$	$0.02221^{+0.00017+0.00034}_{-0.00019-0.00033}$	$0.02209^{+0.00016+0.00030}_{-0.00015-0.00030}$	$0.02196^{+0.00016+0.00032}_{-0.00017-0.00031}$	$0.02199^{+0.00016+0.00031}_{-0.00016-0.00033}$
$100\theta_{MC}$	$1.0328^{+0.0015+0.0027}_{-0.0014-0.0029}$	$1.03081^{+0.00071+0.0017}_{-0.00089-0.0016}$	$1.02676^{+0.00092+0.0015}_{-0.00073-0.0018}$	$1.02759^{+0.00070+0.0014}_{-0.00075-0.0014}$
τ	$0.079^{+0.017+0.034}_{-0.017-0.034}$	$0.086^{+0.017+0.034}_{-0.018-0.033}$	$0.104^{+0.019+0.037}_{-0.019-0.035}$	$0.101^{+0.019+0.035}_{-0.018-0.036}$
n_s	$0.9668^{+0.0086+0.017}_{-0.0083-0.018}$	$0.9774^{+0.0062+0.010}_{-0.0053-0.011}$	$0.9995^{+0.0054+0.012}_{-0.0057-0.011}$	$0.9953^{+0.0054+0.010}_{-0.0055-0.010}$
$\ln(10^{10}A_s)$	$3.095^{+0.035+0.068}_{-0.035-0.068}$	$3.112^{+0.034+0.066}_{-0.036-0.065}$	$3.154^{+0.037+0.073}_{-0.037-0.070}$	$3.147^{+0.037+0.068}_{-0.034-0.069}$
β	$0.209^{+0.045+0.075}_{-0.035-0.077}$	$0.261^{+0.019+0.029}_{-0.012-0.034}$	$0.333^{+0.011+0.022}_{-0.012-0.022}$	$0.320^{+0.011+0.020}_{-0.009-0.020}$
γ	$1.001^{+0.003+0.006}_{-0.003-0.006}$	$1.005^{+0.002+0.003}_{-0.001-0.003}$	$1.013^{+0.001+0.003}_{-0.002-0.003}$	$1.012^{+0.001+0.002}_{-0.001-0.002}$
H_0	$56.1^{+3.4+6.3}_{-3.6-6.1}$	$60.8^{+1.9+2.9}_{-1.4-3.5}$	$70.2^{+1.6+3.7}_{-1.9-3.3}$	$68.2^{+1.4+2.9}_{-1.4-2.8}$
$\chi^2_{\text{best-fit}}$	12962.760	12981.476	14037.120	14059.740

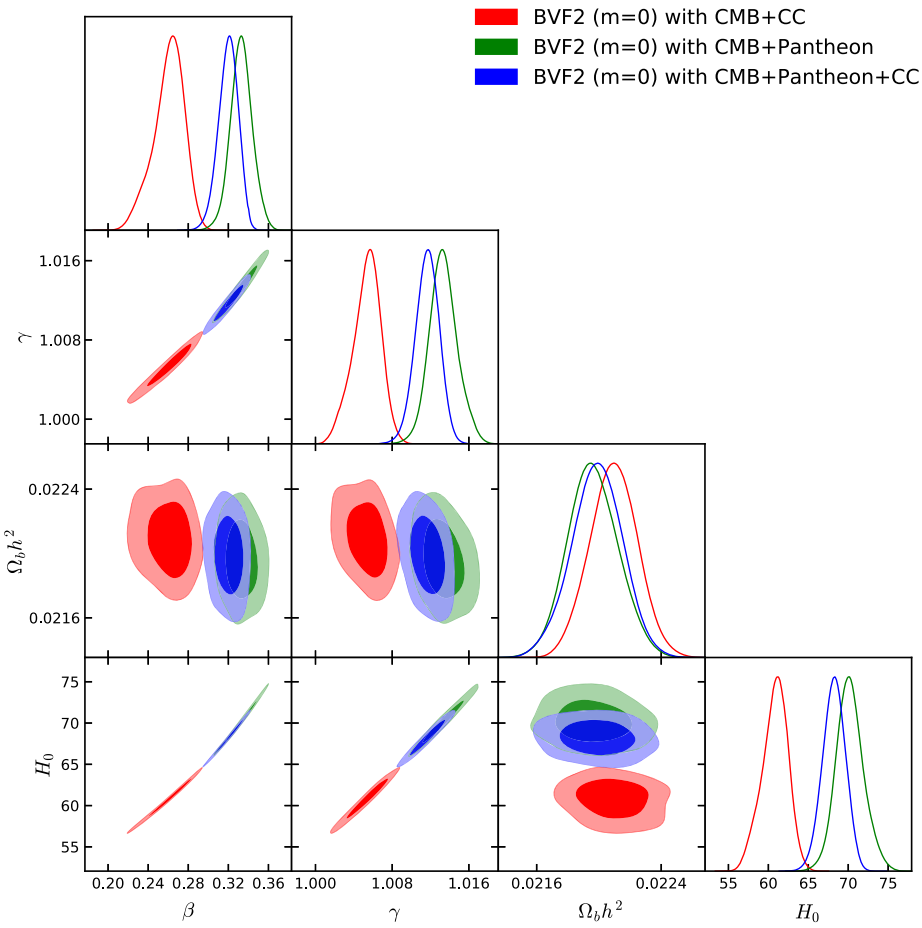

FIG. 9. 68% and 95% C.L. contour plots for the BVF2 model with $m = 0$, using the observational data from different sources. The figure also shows the one-dimensional marginalized posterior distributions for some selected parameters.

addition of external datasets such as CC or Pantheon or both, and moreover, we further note that the strongest constraint on β is achieved for the full combination CMB + Pantheon + CC. To compare the different datasets, we choose the last three, namely, CMB + CC, CMB + Pantheon, and CMB + Pantheon + CC, and in Fig. 9, we show the one-dimensional marginalized posterior distributions for the model parameters as well the contour plots between several combinations of the same free parameters at 68% and 95% C.L. Figure 9 offers some interesting behavior of the parameters. First of all, we can notice also in this case that the addition of Pantheon produces a large shift of the cosmological parameters, now in tension with the estimates obtained by the CMB + CC dataset combination. This shift indicates a disagreement of the Pantheon dataset with the CMB in the context of the BVF model. Second, we find that the parameters H_0, β, and γ have strong positive correlations between them, while the contours of $(\beta, \Omega_b h^2)$ and $(\gamma, \Omega_b h^2)$ are almost vertical, leading to no correlations between them.

Now, concerning the general bulk viscous scenario with free m, we have analyzed it using the same observational datasets such as CMB, CMB + CC, CMB + Pantheon, and CMB + Pantheon + CC, and we present the observational constraints on the model parameters in Table V. From the analyses (refer to Table V), one can see that for the CMB data alone H_0 confirms a lower mean value like in the $m = 0$ case, but with higher error bars, $H_0 = 55.8^{+9.2}_{-9.1}$ (68% C.L., CMB), and again when the external datasets are added, namely, the CMB + CC or CMB + Pantheon or CMB + Pantheon + CC, the error bars are significantly reduced with increased values of the Hubble constant in this way: $H_0 = 65.9^{+3.5}_{-4.0}$ (68% C.L., CMB + CC), $H_0 = 68.0^{+2.7}_{-2.4}$ (68% C.L., CMB + Pantheon), and $H_0 = 68.4^{+1.8}_{-1.5}$ (68% C.L., CMB + Pantheon + CC). While one can recognize that the estimated value of H_0 for the combination CMB + CC is still lower than the Planck estimation [1], interestingly, for the last two datasets, namely, CMB + Pantheon and CMB + Pantheon + CC, we see that, due to larger error bars (which are indeed very small attained for the analysis with CMB alone), the estimated values of H_0 can still catch the local estimation of H_0 by Riess *et al.* in 2019 [82] within 3σ. Eventually, the tension on H_0 is clearly reduced, which is indeed one of the most interesting properties of this bulk viscous model.

TABLE V. 68% and 95% C.L. constraints on various free parameters of the model BVF2 using different observational data. Here, H_0 is in units of km/Mpc/ sec.

Parameters	CMB	CMB + CC	CMB + Pantheon	CMB + Pantheon + CC
$\Omega_b h^2$	$0.02220^{+0.00018+0.00034}_{-0.00018-0.00033}$	$0.02218^{+0.00016+0.00032}_{-0.00016-0.00031}$	$0.02219^{+0.00016+0.00033}_{-0.00017-0.00032}$	$0.02219^{+0.00016+0.00032}_{-0.00016-0.00032}$
$100\theta_{MC}$	$1.0330^{+0.0040+0.0048}_{-0.0040-0.0051}$	$1.0284^{+0.0017+0.0026}_{-0.0014-0.0029}$	$1.0276^{+0.0011+0.0021}_{-0.0012-0.0020}$	$1.02741^{+0.00077+0.0016}_{-0.00083-0.0015}$
τ	$0.078^{+0.021+0.037}_{-0.019-0.039}$	$0.080^{+0.018+0.036}_{-0.019-0.034}$	$0.079^{+0.017+0.033}_{-0.017-0.033}$	$0.078^{+0.017+0.033}_{-0.017-0.033}$
n_s	$0.9670^{+0.0072+0.015}_{-0.0079-0.014}$	$0.9690^{+0.0061+0.0129}_{-0.0062-0.0125}$	$0.9659^{+0.0081+0.014}_{-0.0081-0.0134}$	$0.9668^{+0.0055+0.011}_{-0.0054-0.011}$
$\ln(10^{10}A_s)$	$3.091^{+0.042+0.074}_{-0.037-0.074}$	$3.097^{+0.036+0.068}_{-0.035-0.068}$	$3.093^{+0.034+0.066}_{-0.033-0.067}$	$3.092^{+0.034+0.065}_{-0.033-0.063}$
β	$0.21^{+0.15+0.19}_{-0.15-0.17}$	$0.378^{+0.065+0.097}_{-0.050-0.10}$	$0.427^{+0.020+0.041}_{-0.024-0.038}$	$0.424^{+0.018+0.035}_{-0.017-0.033}$
m	$0.00^{+0.29+0.37}_{-0.17-0.43}$	$-0.35^{+0.21+0.31}_{-0.18-0.31}$	$-0.56^{+0.25+0.31}_{-0.12-0.41}$	$-0.51^{+0.14+0.21}_{-0.09-0.23}$
γ	$1.001^{+0.002+0.005}_{-0.002-0.005}$	$1.002^{+0.002+0.004}_{-0.002-0.004}$	$1.000^{+0.003+0.005}_{-0.003-0.005}$	$1.001^{+0.002+0.003}_{-0.002-0.003}$
H_0	$55.8^{+9.2+11.6}_{-9.1-10.9}$	$66.2^{+3.1+6.2}_{-3.8-5.6}$	$68.0^{+2.7+4.5}_{-2.4-4.7}$	$68.4^{+1.8+3.0}_{-1.5-3.3}$
$\chi^2_{\text{best-fit}}$	12959.084	12977.172	13998.418	14013.918

Let us now focus on the constraints of the other free parameters. From the constraints on γ (see Table V), we see that, this parameter is consistent to 1. The numerical estimations of γ from different observational datasets do not change much from one to another: $\gamma = 1.001^{+0.002}_{-0.002}$ (68% C.L., CMB), $\gamma = 1.002^{+0.001}_{-0.002}$ (68% C.L., CMB + CC), $\gamma = 1.000^{+0.003}_{-0.003}$ (68% C.L., CMB + Pantheon), and $\gamma = 1.001^{+0.002}_{-0.002}$ (68% C.L., CMB + Pantheon + CC). However, significant changes appear in the constraints of the m parameter (let us recall that the m parameter appears from the bulk viscosity: $\eta(\rho_D) = \alpha\rho_D^m$, $\alpha > 0$). From the CMB data alone, we see that $m = 0.00^{+0.29}_{-0.17}$ (68% C.L.), while from the remaining datasets, the mean values of m are negative with increased significance when more datasets are considered: $m = -0.32^{+0.16}_{-0.21}$ (68% C.L., CMB + CC), $m = -0.56^{+0.25}_{-0.12}$ (68% C.L., CMB + Pantheon), and $m = -0.51^{+0.14}_{-0.09}$ (68% C.L., CMB + Pantheon + CC). From all the analyses, we find that $m \neq 0$ at more than 68% C.L., which means it gives a strong indication for a bulk viscous scenario apart from the constant one.

Finally, we discuss the observational bounds on α in terms of the β parameter quantifying the bulk viscosity in the Universe sector. As already reported, the best constraints for β are achieved for the dataset CMB + Pantheon + CC with $\beta = 0.424^{+0.018}_{-0.017}$ at 68% C.L. Thus, overall, we find that the observational data are in support of a bulk viscous cosmology. We close this section with Fig. 10, in which, for the last three best analyses, namely, CMB + CC, CMB + Pantheon, and CMB + Pantheon + CC, we display the one-dimensional marginalized posterior distributions for the free parameters of the model as well as the contour plots between various combinations of the model parameters at 68% and 95% C.L. From this figure (i.e., Fig. 10), we clearly see that the parameter m has a strong positive correlation to γ and β has a negative correlation to both m and γ, partially broken by the addition of the Pantheon dataset. Moreover, the parameter m presents a positive correlation with H_0 for the CMB + CC case, while the addition of the Pantheon dataset changes the direction of the correlation. This is the reason why by adding the Pantheon dataset the H_0 value is very well constrained, shifting m toward negative values. In Fig. 10, all the bounds are now very well consistent, and therefore we can conclude that having a negative m parameter is a way to solve the disagreement between the CMB and Pantheon datasets we saw in Fig. 9. The full combination of datasets considered in this work is therefore converging to a concordance model with a negative m at several standard deviations, a larger β different from zero, a γ consistent with 1, a larger value for the Hubble constant, and a smaller value for θ_{MC}. For this model, we gain a $\Delta\chi^2 = 46$ with respect to the same case with $m = 0$.

1. BVF2 model at large scales

We continue by discussing the effects on the CMB TT and matter power spectra for the two variations of this bulk viscous scenario, namely, for $m = 0$ and with free m.

As far as the simplest case with the constant bulk viscous model (i.e., $m = 0$) is concerned, in Fig. 11, we plot the CMB TT spectra. To draw the plot, we have used the best-fit values of the model parameters obtained from all the observational datasets that we have used in this work. From Fig. 11, we find that at lower multipoles (i.e., $l \leq 10$) a mild deviation in the curves for CMB and CMB + CC appear, compared to the curves for CMB + Pantheon and CMB + Pantheon + CC. However, for higher multipoles, we cannot distinguish between the curves. Finally, we consider the general scenario with m as a free parameter and plot the CMB TT spectra in Fig. 12 using the best-fit values of the parameters from all the observational datasets. We notice that, compared to the previous case (BVF2 with $m = 0$), the CMB TT spectra exhibit similar features.

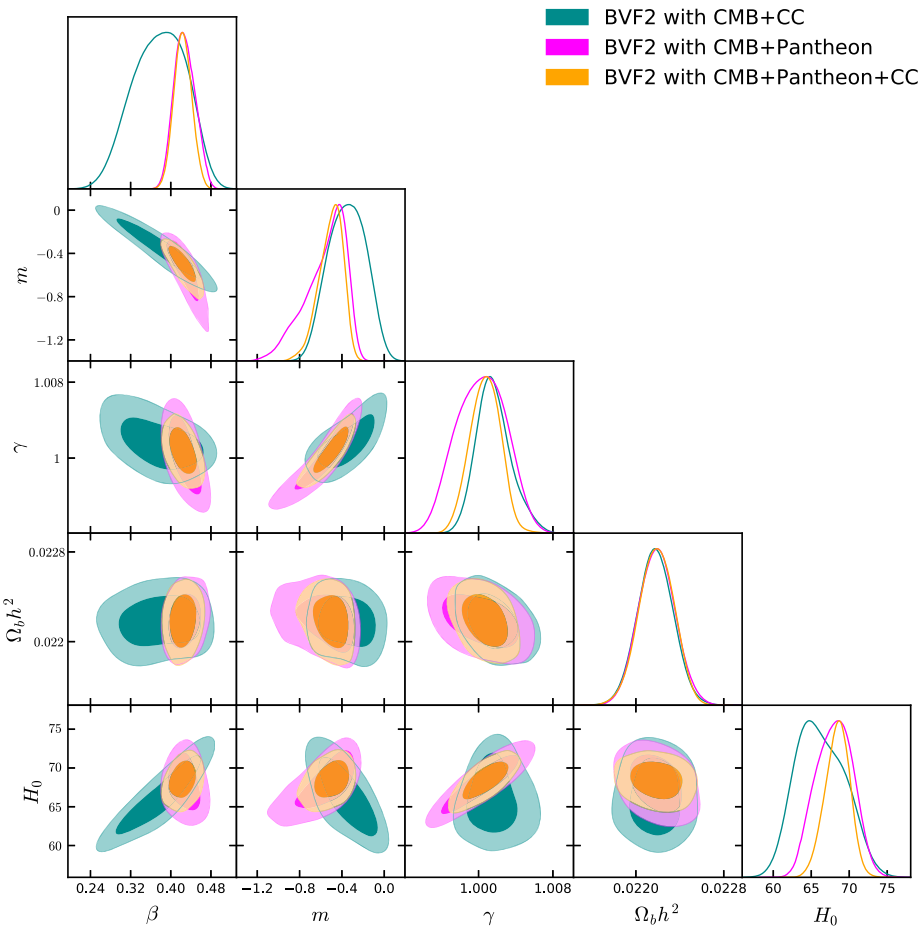

FIG. 10. The figure displays the 68% and 95% C.L. contour plots between various combinations of the parameters of the model BVF2 using the observational data from different sources. The figure also shows the one-dimensional marginalized posterior distributions for some selected parameters.

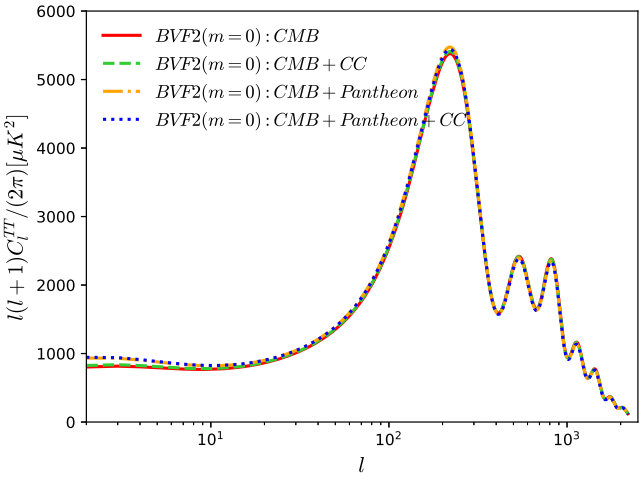

FIG. 11. We show the CMB TT spectra for the BVF2 model with $m = 0$ using the best-fit values of the free and derived parameters.

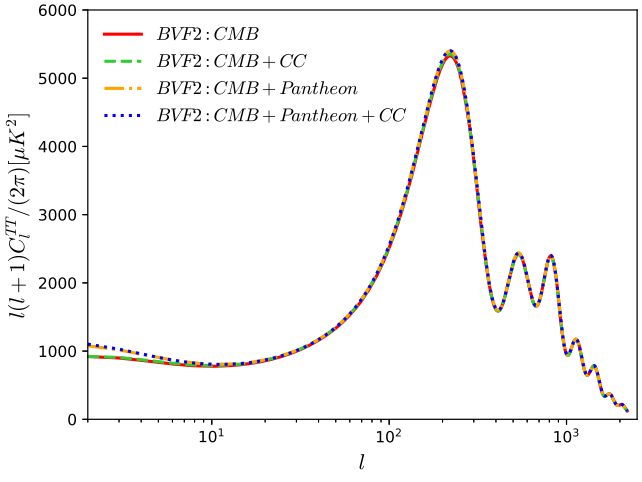

FIG. 12. Temperature anisotropy in the CMB spectra for different best-fit values of the free and derived parameters of the generalized bulk viscous scenario BVF2.

TABLE VI. The table displays the values of $\ln B_{ij}$ for all the observational datasets and for all variants of the bulk viscous models. Here, $\ln B_{ij} = \ln B_i - \ln B_j$ (i represents the reference model ΛCDM, and j is for the underlying model).

Dataset	Model	$\ln B_{ij}$
CMB	BVF1 ($m = 0$)	3.4
CMB + CC	BVF1 ($m = 0$)	5.7
CMB + Pantheon	BVF1 ($m = 0$)	2.6
CMB + Pantheon + CC	BVF1 ($m = 0$)	2.9
CMB	BVF1 (m free)	5.1
CMB + CC	BVF1 (m free)	7
CMB + Pantheon	BVF1 (m free)	2.9
CMB + Pantheon + CC	BVF1 (m free)	3.6
CMB	BVF2 ($m = 0$)	4.7
CMB + CC	BVF2 ($m = 0$)	7.2
CMB + Pantheon	BVF2 ($m = 0$)	3.6
CMB + Pantheon + CC	BVF2 ($m = 0$)	4.3
CMB	BVF2 (m free)	6.6
CMB + CC	BVF2 (m free)	9.1
CMB + Pantheon	BVF2 (m free)	4.1
CMB + Pantheon + CC	BVF2 (m free)	5.2

C. Bayesian evidence

In the previous subsections, we have mainly focused on the observational constraints extracted from different variants of the bulk viscous scenarios. An important question that naturally arises in this context is how efficient the present bulk viscous models are compared to the standard ΛCDM model. The answer can be found by calculating the Bayesian evidence values of the bulk viscous models with respect to this standard ΛCDM model. The calculation can be done through the publicly available code MCEvidence [83,84].[2] Now, one can introduce the so-called Jeffreys scale that quantifies the strength of evidence of the underlying model against the reference model. The Jeffreys scale deals with the values of $\ln B_{ij}$, where B_ij is the Bayesian evidence of the reference scenario ΛCDM (M_i), with respect to the bulk viscous cosmic model (M_j) [85]. For $0 \leq \ln B_{ij} < 1$, weak evidence; for $1 \leq \ln B_{ij} < 3$, definite/positive evidence; for $3 \leq \ln B_{ij} < 5$, strong evidence; and for $\ln B_{ij} \geq 5$, very strong evidence for the ΛCDM model against the bulk viscous scenario is signaled. Following Refs. [83,84], we computed the values of $\ln B_{ij}$ for all such variants of the bulk viscous model with respect to the ΛCDM model. The values of $\ln B_{ij}$ are summarized in Table VI for all possible observational datsets. From Table VI, it is clear that ΛCDM is favored over the bulk viscous scenarios.

[2]One can freely access this code from the link github.com/yabebalFantaye/MCEvidence.

IV. CONCLUSIONS

We have considered a unified dark fluid endowed with bulk viscosity in a spatially flat FLRW universe where the coefficient of the bulk viscosity has a power law evolution: $\eta(\rho_D) = \alpha\rho_d^m$ ($\alpha > 0$ and m is a free parameter) and $p_D = (\gamma - 1)\rho_D$, $\gamma \in \mathbb{R}$ being the barotropic state parameter. So, one can realize that the above choice for the bulk viscous coefficient automatically includes a number of models, specifically models with fixed m. For $\gamma = 1$, we rename the scenario BVF1, while for free γ, we recognize the bulk viscous scenario as BVF2. For $m = 0$, one can realize a constant bulk viscous model. Thus, to include the specific cases with $m = 0$, both the scenarios (i.e., BVF1 and BVF2) have been further classified as i) the case with $m = 0$ [BVF1 ($m = 0$), BVF2 ($m = 0$)], representing the constant bulk viscous scenario, and ii) the case for free m [BVF1 (m: free), BVF2 (m: free)], which is the most general bulk viscous scenario in this work. Thus, essentially, we consider four different bulk viscous scenarios and constrain all of them using the observational datasets from the CMB, Pantheon sample of supernovae type Ia, and the Hubble parameter measurements from the cosmic chronometers.

For the constant bulk viscous scenarios BVF1 ($m = 0$) and BVF2 ($m = 0$), the results of which are summarized in Tables II and IV, respectively, we find that the parameter β quantifying the observational evidence of the bulk viscosity is strictly nonzero at several standard deviations. The model BVF2 ($m = 0$) has an additional observational feature that is absent in BVF1 ($m = 0$). We find that for the combinations CMB + Pantheon and CMB + Pantheon + CC the tension on H_0 is released within 3σ. In fact, the combination CMB + Pantheon is very effective in reconciling this tension (see Table IV).

Concerning the general bulk viscous scenarios with free m parameter, the results are summarized in Table III (BVF1 with free m) and Table V (BVF2 with free m). For BVF1 (m free), we find a strong anticorrelation between the free parameter m and the quantifying bulk viscous parameter β. Precisely, we find that β is nonzero at more than two standard deviations for all the datasets. Regarding the m parameter, although for CMB alone $m = 0$ is allowed within 68% C.L., for other datasets, $m \neq 0$ becomes strongest. In addition, we see that the inclusion of Pantheon to CMB weakly reduces the tension on H_0. For the BVF2 (m free) scenario, we have observations similar to those for BVF1 (m free). We find that, although for CMB-alone data $m = 0$ is certainly the case, for other datasets, $m \neq 0$ is strongly preferred. The parameter β quantifying the bulk viscosity in the Universe, we find its positive evidence for all the observational datasets at more than two standard deviations. Additionally, for the CMB + Pantheon and CMB + Pantheon + CC datasets, this specific bulk viscous scenario has the ability to reduce the H_0 tension weakly. Thus, considering the observational limits on both β and m for both BVF1 and BVF2, a strong

indication of a nonzero bulk viscous scenario (since $\beta \neq 0$) apart from the constant bulk viscous coefficient (since $m \neq 0$ except for CMB alone) is supported. We also perform Bayesian evidence analyses for all the bulk viscous scenarios shown in Table VI aiming to compared them with respect to the standard ΛCDM model. Our analyses report that ΛCDM is favored over the bulk viscous scenarios, at least for the employed observational datasets.

To conclude, perhaps along with other findings, the best finding is to explore the ability of the bulk viscous scenarios to reduce the H_0 tension weakly. We use "weakly" in the sense that the tension is released under 3σ C.L. In summary, we see that the bulk viscous scenarios might be able to compete with other cosmological models in which an additional constraint in terms of either the inclusion of phantom dark energy equation of state [86–90] or the nonzero interaction [91–95] is necessary to release the H_0 tension.

ACKNOWLEDGMENTS

The authors thank the referee for some essential comments that helped us improve the manuscript. The authors also thank Professor J. D. Barrow for some very useful discussions while working on this article. W. Y. has been supported by the National Natural Science Foundation of China under Grants No. 11705079 and No. 11647153. S. P. has been supported by the Mathematical Research Impact-Centric Support Scheme (MATRICS), File No. MTR/2018/000940, given by the Science and Engineering Research Board (SERB), Government of India. S. P. also acknowledges partial support from the Faculty Research and Development Fund (FRPDF) Scheme of Presidency University, Kolkata, India. E. D. V. acknowledges the support from the European Research Council in the form of a Consolidator Grant with Grant No. 681431. J. L. was supported by the National Natural Science Foundation of China under Grant No. 11645003.

[1] P. A. R. Ade *et al.* (Planck Collaboration), Planck 2015 results. XIII. Cosmological parameters, Astron. Astrophys. **594**, A13 (2016).
[2] E. J. Copeland, M. Sami, and S. Tsujikawa, Dynamics of dark energy, Int. J. Mod. Phys. D **15**, 1753 (2006).
[3] Y. L. Bolotin, A. Kostenko, O. A. Lemets, and D. A. Yerokhin, Cosmological evolution with interaction between dark energy and dark matter, Int. J. Mod. Phys. D **24**, 1530007 (2015).
[4] S. Chaplygin, Sci. Mem. Moscow Univ. Math. Phys. **21**, 1 (1904).
[5] N. Bilic, G. B. Tupper, and R. D. Viollier, Unification of dark matter and dark energy: The inhomogeneous Chaplygin gas, Phys. Lett. B **535**, 17 (2002).
[6] A. Y. Kamenshchik, U. Moschella, and V. Pasquier, An alternative to quintessence, Phys. Lett. B **511**, 265 (2001).
[7] V. Gorini, A. Kamenshchik, and U. Moschella, Can the Chaplygin gas be a plausible model for dark energy?, Phys. Rev. D **67**, 063509 (2003).
[8] V. Gorini, A. Kamenshchik, U. Moschella, V. Pasquier, and A. Starobinsky, Stability properties of some perfect fluid cosmological models, Phys. Rev. D **72**, 103518 (2005).
[9] M. C. Bento, O. Bertolami, and A. A. Sen, Generalized Chaplygin gas, accelerated expansion and dark energy matter unification, Phys. Rev. D **66**, 043507 (2002).
[10] J. Lu, Y. Gui, and L. X. Xu, Observational constraint on generalized Chaplygin gas model, Eur. Phys. J. C **63**, 349 (2009).
[11] L. Xu, J. Lu, and Y. Wang, Revisiting generalized Chaplygin gas as a unified dark matter and dark energy model, Eur. Phys. J. C **72**, 1883 (2012).
[12] H. B. Benaoum, Accelerated universe from modified Chaplygin gas and tachyonic fluid, arXiv:hep-th/0205140.
[13] U. Debnath, A. Banerjee, and S. Chakraborty, Role of modified Chaplygin gas in accelerated universe, Classical Quantum Gravity **21**, 5609 (2004).
[14] J. Lu, L. Xu, J. Li, B. Chang, Y. Gui, and H. Liu, Constraints on modified Chaplygin gas from recent observations and a comparison of its status with other models, Phys. Lett. B **662**, 87 (2008).
[15] L. Xu, Y. Wang, and H. Noh, Modified Chaplygin gas as a unified dark matter and dark energy model and cosmic constraints, Eur. Phys. J. C **72**, 1931 (2012).
[16] H. Hova and H. Yang, A dark energy model alternative to generalized Chaplygin gas, Int. J. Mod. Phys. D **27**, 1750178 (2018).
[17] A. Hernandez-Almada, J. Magana, M. A. Garcia-Aspeitia, and V. Motta, Cosmological constraints on alternative model to Chaplygin fluid revisited, Eur. Phys. J. C **79**, 12 (2019).
[18] W. Yang, S. Pan, A. Paliathanasis, S. Ghosh, and Y. Wu, Observational constraints of a new unified dark fluid and the H_0 tension, arXiv:1904.10436 [Mon. Not. R. Astron. Soc. (to be published)].
[19] J. D. Barrow, Graduated inflationary Universes, Phys. Lett. B **235**, 40 (1990).
[20] J. D. Barrow, String-driven inflationary and deflationary cosmological models, Nucl. Phys. **B310**, 743 (1988).
[21] J. D. Barrow, The deflationary Universe: An instability of the de Sitter Universe, Phys. Lett. B **180**, 335 (1986).
[22] D. Pavón, J. Bafaluy, and D. Jou, Causal Friedmann-Robertson-Walker cosmology, Classical Quantum Gravity **8**, 347 (1991).
[23] W. Zimdahl, Bulk viscous cosmology, Phys. Rev. D **53**, 5483 (1996).
[24] A. A. Coley, R. J. van den Hoogen, and R. Maartens, Qualitative viscous cosmology, Phys. Rev. D **54**, 1393 (1996).

[25] V. R. Gavrilov, V. N. Melnikov, and R. Triay, Exact solutions in multidimensional cosmology with shear and bulk viscosity, Classical Quantum Gravity **14**, 2203 (1997).
[26] L. P. Chimento, A. S. Jakubi, V. Mendez, and R. Maartens, Cosmological solutions with nonlinear bulk viscosity, Classical Quantum Gravity **14**, 3363 (1997).
[27] J. A. Belinchon, Cosmological models with bulk viscosity in presence of adiabatic matter creation and with G, c and Lambda variables, Gen. Relativ. Gravit. **32**, 1487 (2000).
[28] J. A. Belinchon, T. Harko, and M. K. Mak, Causal bulk viscous cosmology: Renormalization group, dimensional analysis and structural stability theory approach, Classical Quantum Gravity **19**, 3003 (2002).
[29] M. K. Mak and T. Harko, Bianchi type I universes with causal bulk viscous cosmological fluid, Int. J. Mod. Phys. D **11**, 447 (2002).
[30] I. H. Brevik and S. D. Odintsov, On the Cardy-Verlinde entropy formula in viscous cosmology, Phys. Rev. D **65**, 067302 (2002).
[31] M. K. Mak, J. A. Belinchon, and T. Harko, Causal bulk viscous dissipative isotropic cosmologies with variable gravitational and cosmological constants, Int. J. Mod. Phys. D **11**, 1265 (2002).
[32] M. K. Mak and T. Harko, Bulk viscous Brans-Dicke cosmological models and late-time acceleration of the universe, Int. J. Mod. Phys. D **12**, 925 (2003).
[33] I. H. Brevik and O. Gorbunova, Dark energy and viscous cosmology, Gen. Relativ. Gravit. **37**, 2039 (2005).
[34] M. Giovannini, Cosmological perturbations for imperfect fluids, Classical Quantum Gravity **22**, 5243 (2005).
[35] M. Giovannini, Interacting viscous mixtures, Phys. Lett. B **622**, 349 (2005).
[36] M. Cataldo, N. Cruz, and S. Lepe, Viscous dark energy and phantom evolution, Phys. Lett. B **619**, 5 (2005).
[37] J. C. Fabris, S. V. B. Goncalves, and R. de Sa Ribeiro, Bulk viscosity driving the acceleration of the Universe, Gen. Relativ. Gravit. **38**, 495 (2006).
[38] M. G. Hu and X. H. Meng, Bulk viscous cosmology: Statefinder and entropy, Phys. Lett. B **635**, 186 (2006).
[39] R. Colistete, J. C. Fabris, J. Tossa, and W. Zimdahl, Bulk viscous cosmology, Phys. Rev. D **76**, 103516 (2007).
[40] A. Avelino and U. Nucamendi, Can a matter-dominated model with constant bulk viscosity drive the accelerated expansion of the universe?, J. Cosmol. Astropart. Phys. 04 (2009) 006.
[41] B. Li and J. D. Barrow, Does bulk viscosity create a viable unified dark matter model?, Phys. Rev. D **79**, 103521 (2009).
[42] W. S. Hipolito-Ricaldi, H. E. S. Velten, and W. Zimdahl, Non-adiabatic dark fluid cosmology, J. Cosmol. Astropart. Phys. 06 (2009) 016.
[43] H. Velten and D. J. Schwarz, Constraints on dissipative unified dark matter, J. Cosmol. Astropart. Phys. 09 (2011) 016.
[44] J. S. Gagnon and J. Lesgourgues, Dark goo: Bulk viscosity as an alternative to dark energy, J. Cosmol. Astropart. Phys. 09 (2011) 026.
[45] I. Brevik, E. Elizalde, S. Nojiri, and S. D. Odintsov, Viscous little rip cosmology, Phys. Rev. D **84**, 103508 (2011).
[46] B. Pourhassan, Viscous modified cosmic Chaplygin gas cosmology, Int. J. Mod. Phys. D **22**, 1350061 (2013).
[47] A. Avelino, R. Garcia-Salcedo, T. Gonzalez, U. Nucamendi, and I. Quiros, Bulk viscous matter-dominated Universes: Asymptotic properties, J. Cosmol. Astropart. Phys. 08 (2013) 012.
[48] A. Avelino, Y. Leyva, and L. A. Urena-Lopez, Interacting viscous dark fluids, Phys. Rev. D **88**, 123004 (2013).
[49] H. Velten, J. Wang, and X. Meng, Phantom dark energy as an effect of bulk viscosity, Phys. Rev. D **88**, 123504 (2013).
[50] M. M. Disconzi, T. W. Kephart, and R. J. Scherrer, New approach to cosmological bulk viscosity, Phys. Rev. D **91**, 043532 (2015).
[51] B. Mostaghel, H. Moshafi, and S. M. S. Movahed, Non-minimal derivative coupling scalar field and bulk viscous dark energy, Eur. Phys. J. C **77**, 541 (2017).
[52] C. M. S. Barbosa, H. Velten, J. C. Fabris, and R. O. Ramos, Assessing the impact of bulk and shear viscosities on large scale structure formation, Phys. Rev. D **96**, 023527 (2017).
[53] J. Haro and S. Pan, Bulk viscous quintessential inflation, Int. J. Mod. Phys. D **27**, 1850052 (2018).
[54] A. Sasidharan, N. D. J. Mohan, M. V. John, and T. K. Mathew, Bayesian analysis of bulk viscous matter dominated universe, Eur. Phys. J. C **78**, 628 (2018).
[55] I. Brevik, Ø. Grøn, J. de Haro, S. D. Odintsov, and E. N. Saridakis, Viscous cosmology for early- and late-time Universe, Int. J. Mod. Phys. D **26**, 1730024 (2017).
[56] S. Chakraborty, Is emergent Universe a consequence of particle creation process?, Phys. Lett. B **732**, 81 (2014).
[57] S. Chakraborty, S. Pan, and S. Saha, A third alternative to explain recent observations: Future deceleration, Phys. Lett. B **738**, 424 (2014).
[58] S. Pan and S. Chakraborty, Will there be future deceleration? A study of particle creation mechanism in non-equilibrium thermodynamics, Adv. High Energy Phys. **2015**, 1 (2015).
[59] R. C. Nunes and D. Pavón, Phantom behavior via cosmological creation of particles, Phys. Rev. D **91**, 063526 (2015).
[60] J. A. S. Lima, R. C. Santos, and J. V. Cunha, Is ΛCDM an effective CCDM cosmology?, J. Cosmol. Astropart. Phys. 03 (2016) 027.
[61] J. de Haro and S. Pan, Gravitationally induced adiabatic particle production: From big bang to de Sitter, Classical Quantum Gravity **33**, 165007 (2016).
[62] S. Pan, J. de Haro, A. Paliathanasis, and R. J. Slagter, Evolution and dynamics of a matter creation model, Mon. Not. R. Astron. Soc. **460**, 1445 (2016).
[63] R. C. Nunes and S. Pan, Cosmological consequences of an adiabatic matter creation process, Mon. Not. R. Astron. Soc. **459**, 673 (2016).
[64] R. C. Nunes, Connecting inflation with late cosmic acceleration by particle production, Int. J. Mod. Phys. D **25**, 1650067 (2016).
[65] R. C. Nunes, Gravitationally induced particle production and its impact on structure formation, Gen. Relativ. Gravit. **48**, 107 (2016).
[66] A. Paliathanasis, J. D. Barrow, and S. Pan, Cosmological solutions with gravitational particle production and nonzero curvature, Phys. Rev. D **95**, 103516 (2017).

[67] L. Aresté Saló and J. de Haro, Cosmological solutions in spatially curved universes with adiabatic particle production, Classical Quantum Gravity **34**, 065001 (2017).
[68] S. Pan, B. Kumar Pal, and S. Pramanik, Gravitationally influenced particle creation models and late-time cosmic acceleration, Int. J. Geom. Methods Mod. Phys. **15**, 1850042 (2018).
[69] S. Pan, J. D. Barrow, and A. Paliathanasis, Two-fluid solutions of particle-creation cosmologies, Eur. Phys. J. C **79**, 115 (2019).
[70] J. A. S. Lima and A. S. M. Germano, On the equivalence of matter creation in cosmology, Phys. Lett. A **170**, 373 (1992).
[71] A. G. Riess *et al.* (Supernova Search Team), Type Ia supernova discoveries at $z > 1$ from the Hubble Space Telescope: Evidence for past deceleration and constraints on dark energy evolution, Astrophys. J. **607**, 665 (2004).
[72] Y. Wang and P. Mukherjee, Robust dark energy constraints from supernovae, galaxy clustering, and three-year wilkinson microwave anisotropy probe observations, Astrophys. J. **650**, 1 (2006).
[73] W. Hu, Structure formation with generalized dark matter, Astrophys. J. **506**, 485 (1998).
[74] R. Adam *et al.* (Planck Collaboration), Planck 2015 results. I. Overview of products and scientific results, Astron. Astrophys. **594**, A1 (2016).
[75] N. Aghanim *et al.* (Planck Collaboration), Planck 2015 results. XI. CMB power spectra, likelihoods, and robustness of parameters, Astron. Astrophys. **594**, A11 (2016).
[76] D. M. Scolnic *et al.*, The complete light-curve sample of spectroscopically confirmed SNe Ia from Pan-STARRS1 and cosmological constraints from the combined pantheon sample, Astrophys. J. **859**, 101 (2018).
[77] M. Moresco, L. Pozzetti, A. Cimatti, R. Jimenez, C. Maraston, L. Verde, D. Thomas, A. Citro, R. Tojeiro, and D. Wilkinson, A 6% measurement of the Hubble parameter at $z \sim 0.45$: Direct evidence of the epoch of cosmic reacceleration, J. Cosmol. Astropart. Phys. 05 (2016) 014.
[78] A. Lewis and S. Bridle, Cosmological parameters from CMB and other data: A Monte Carlo approach, Phys. Rev. D **66**, 103511 (2002).
[79] A. Gelman and D. Rubin, Inference from iterative simulation using multiple sequences, Stat. Sci. **7**, 457 (1992).
[80] A. G. Riess *et al.*, A 2.4% determination of the local value of the Hubble constant, Astrophys. J. **826**, 56 (2016).
[81] A. G. Riess *et al.*, New parallaxes of Galactic cepheids from spatially scanning the Hubble Space Telescope: Implications for the Hubble constant, Astrophys. J. **855**, 136 (2018).
[82] A. G. Riess, S. Casertano, W. Yuan, L. M. Macri, and D. Scolnic, Large magellanic cloud cepheid standards provide a 1% foundation for the determination of the Hubble constant and stronger evidence for physics beyond ΛCDM, Astrophys. J. **876**, 85 (2019).
[83] A. Heavens, Y. Fantaye, A. Mootoovaloo, H. Eggers, Z. Hosenie, S. Kroon, and E. Sellentin, Marginal likelihoods from Monte Carlo Markov chains, arXiv:1704.03472.
[84] A. Heavens, Y. Fantaye, E. Sellentin, H. Eggers, Z. Hosenie, S. Kroon, and A. Mootoovaloo, No Evidence for Extensions to the Standard Cosmological Model, Phys. Rev. Lett. **119**, 101301 (2017).
[85] R. E. Kass and A. E. Raftery, Bayes factors, J. Am. Stat. Assoc. **90**, 773 (1995).
[86] E. Di Valentino, A. Melchiorri, and J. Silk, Reconciling Planck with the local value of H_0 in extended parameter space, Phys. Lett. B **761**, 242 (2016).
[87] E. Di Valentino, A. Melchiorri, E. V. Linder, and J. Silk, Constraining dark energy dynamics in extended parameter space, Phys. Rev. D **96**, 023523 (2017).
[88] E. Di Valentino, E. V. Linder, and A. Melchiorri, Vacuum phase transition solves the H_0 tension, Phys. Rev. D **97**, 043528 (2018).
[89] S. Vagnozzi, S. Dhawan, M. Gerbino, K. Freese, A. Goobar, and O. Mena, Constraints on the sum of the neutrino masses in dynamical dark energy models with $w(z) \geq -1$ are tighter than those obtained in ΛCDM, Phys. Rev. D **98**, 083501 (2018).
[90] W. Yang, S. Pan, E. Di Valentino, E. N. Saridakis, and S. Chakraborty, Observational constraints on one-parameter dynamical dark-energy parametrizations and the H_0 tension, Phys. Rev. D **99**, 043543 (2019).
[91] S. Kumar and R. C. Nunes, Echo of interactions in the dark sector, Phys. Rev. D **96**, 103511 (2017).
[92] E. Di Valentino, A. Melchiorri, and O. Mena, Can interacting dark energy solve the H_0 tension?, Phys. Rev. D **96**, 043503 (2017).
[93] W. Yang, S. Pan, E. Di Valentino, R. C. Nunes, S. Vagnozzi, and D. F. Mota, Tale of stable interacting dark energy, observational signatures, and the H_0 tension, J. Cosmol. Astropart. Phys. 09 (2018) 019.
[94] W. Yang, A. Mukherjee, E. Di Valentino, and S. Pan, Interacting dark energy with time varying equation of state and the H_0 tension, Phys. Rev. D **98**, 123527 (2018).
[95] S. Pan, W. Yang, C. Singha, and E. N. Saridakis, Observational constraints on sign-changeable interaction models and alleviation of the H_0 tension, arXiv:1903.10969.